JOURNAL OF MATERIALS SCIENCE **34** (1999) 4163–4172

Damage monitoring of carbon fiber-reinforced plastics with Michelson interferometric fiber-optic sensors

H. TSUDA, J. TAKAHASHI, K. URABE
Department of Composite Materials, National Institute of Materials and Chemical Research, Agency of Industrial Science and Technology, Ministry of International Trade and Industry, Tsukuba 305-8565, Japan

T. IKEGUCHI*
University of Tsukuba, Tsukuba 305-8573, Japan
E-mail: tsuda@nimc.go.jp

This paper presents the application of a Michelson interferometric fiber-optic sensor for monitoring the damage of fiber-reinforced plastics. A Michelson interferometric fiber-optic sensor was mounted on the surface of unidirectionally aligned carbon fiber-reinforced epoxy composites. Response of the interference signal to either dynamic or static loading was investigated. Specimen being impacted, the optical interference signal dropped suddenly and then oscillated. The tensile test was performed with the measurement of optical interference signal, strain as well as acoustic emission. Both fast Fourier transform and digital filter processing of the optical interference signal were carried out to characterize the damage signal from the fiber-optic sensor. The optical interference signal whose frequency ranged from tens to hundreds Hz occurred when the specimen was damaged. It was shown that real-time information comparable to acoustic emission (AE) data could be obtained from Michelson interferometric fiber-optic sensor through a digital filtering technique. The Michelson interferometric fiber-optic sensor proved to be effective for monitoring the damage processes of the material studied.

1. Introduction

Fiber-reinforced plastics (FRP) have been widely used as structural materials for aerospace and automobile applications because of their superior specific strength and rigidity. As the application of FRP broadens, the real-time monitoring of its structural integrity has been desired. It has been recently paid much attention to the material system in which damage occurrence is monitored with sensors and damage propagation is controlled with actuators. Such material systems are called "smart materials" [1, 2]. Fiber-optic sensors have been promising sensors used in smart materials. This is because fiber-optic sensors are lightweight, immune to electromagnetic interference, and can measure various physical parameters using one probe.

Several studies of damage detection for FRP with optical fibers have been reported [3–10]. Hofer and other researchers have demonstrated that optical fiber systems are capable of monitoring the damage in composite materials [3–7]. They indicated that damage in composite materials could be detected by the fracture of embedded optical fibers. The intensity of the light propagating through an optical fiber drops substantially whenever a fiber is broken. By monitoring the light transmitted through the fiber, the damage state of the host material can be determined. While this technique was shown to be successful, the sensitivity of damage detection was insufficient owing to high strength of optical fibers. Kwon *et al*. have detected the matrix crack initiation of cross-ply composites with an embedded Michelson interferometric fiber-optic sensor during four-point bending tests [9]. They indicated that the high-frequency interference signal resulted from matrix cracking. Matrix cracking was sensed by processing the optical interference signal. In their study, however, the extent of damage monitoring was limited to only matrix cracking.

Embedment of fiber-optic sensors in composite materials causes a decrease in strength of not only sensors themselves but also host materials. The diameter of the optical fiber is over 100 μm although that of the reinforcing fiber is usually about 10 μm. Embedded optical fibers behave as defects in host materials. From the reliability point of view, a mounted-type sensor is

* *Present address*: Toyota Motor Co. Ltd., Toyota 473-0938, Japan.

preferable. The purpose of the present study is damage monitoring of FRP with a mounted-type Michelson interferometric fiber-optic sensor under dynamic and static loading conditions. Unidirectionally aligned carbon fiber-reinforced epoxy composites were used as monitored materials. An impulse was provided with a hammer used for the Charpy impact test and the response of the optical interference signal to impulse was investigated. During the tensile test, the optical interference signal, strain as well as acoustic emission (AE) were measured. In order to characterize the damage signal from the fiber-optic sensor, a comparison was made between the optical interference signal and damage state evaluated from strain and AE data.

2. Experimental

2.1. Principles of damage monitoring

Consider the case where coherent light of angular frequency, ω, is launched into two single-mode optical fibers. One fiber is strained, and the other is maintained in a strain-free state. The strained and strain-free fibers are called the sensing and the reference fibers, respectively. Output from the sensing fiber, A_s, and that from the reference fiber, A_r are expressed by Equations 1 and 2, respectively.

$$A_s = |A_s| \exp\{i(\omega t + \phi_s)\} \quad (1)$$

$$A_r = |A_r| \exp\{i(\omega t + \phi_r)\} \quad (2)$$

where $|A|$, t and ϕ denote the amplitude, time and phase, respectively. The intensity of the signal combined the light in a sensing fiber with that in a reference fiber, $|A_s + A_r|^2$, is given by Equation 3

$$\begin{aligned} |A_s + A_r|^2 &= (A_s + A_r)(\overline{A_s + A_r}) \\ &= |A_s|^2 + |A_r|^2 + 2|A_s||A_r| \cos(\phi_s - \phi_r) \end{aligned} \quad (3)$$

where $\overline{A_s + A_r}$ denotes the conjugate complex of $A_s + A_r$. The last term in Equation 3 represents the interference component. The change in optical path length is associated with the phase shift in the interference signal. When the sensing fiber with a gauge length, L, is strained along the fiber axis by ε_z, the induced phase shift, $\Delta\Phi$, in the interference signal can be expressed by Equation 4 [11].

$$|\Delta\phi| = \frac{2\pi n L}{\lambda} \left\{ 1 - \frac{n^2}{2}[P_{12} - \nu(P_{11} + P_{12})] \right\} |\varepsilon_z| \quad (4)$$

where n, ν and P_{ij} denote the refractive index, Poisson's ratio and strain-optic coefficients, respectively, of the optical fiber, and λ is the wavelength of the light source. The optical and mechanical properties of the optical fiber employed in the present study are listed in Table I [12].

As can be seen from Equation 4, it cannot distinguish whether the phase shift in the interference signal is induced by tension or compression. The interference signal changes discontinuously when the sensor detects the vibration. Damage in FRP, such as matrix cracking and fiber breaking, is considered to induce vibration by releasing the strain energy. Thus, damage can be detected from the waveform of the interference signal.

TABLE I Optical and mechanical properties of the optical fiber employed

Refractive index, n	1.46
Poisson's ratio, ν	0.17
Strain-optic coefficients,	
P_{11}	0.11
P_{12}	0.25

2.2. Measuring system

An experimental setup of the employed system including the Michelson interferometer is shown in Fig. 1. Monitored materials were 12-ply unidirectional carbon fiber-reinforced epoxy composites (T700/#2500, Toray). A He-Ne laser whose wavelength is 633 nm was used as the light source. The laser beam was launched into a 2 × 2 coupler which splits the light into both the sensing and the reference fibers. The sensing fiber was mounted on the specimen along the reinforcing fiber axis with cyanoacrylate adhesive. The reference fiber was maintained in a strain-free state. Conductive paste was painted on the end of both the sensing and the reference fibers in order to enhance the reflection efficiency. The reflected beams of light were combined through the 2 × 2 coupler. The interference signal was converted to voltage with a photodiode.

Optical fibers consist of the core, cladding and coating. The light propagating in an optical fiber is trapped within the core because of the total reflection at the core-cladding interface. In the sensing part of the sensing fiber, the coating was stripped so that the core in which the light traveled could be strained as much as the tested specimen. The sensor length, ΔL, was controlled with a Teflon sheet as shown in Fig. 2. For the Michelson interferometric fiber-optic sensor, the gauge length, L, of the sensor is twice the sensor length, ΔL. This is because the light is propagated back and forth in the fiber by reflection on the fiber end.

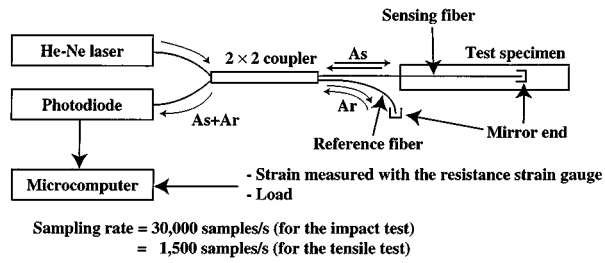

Figure 1 An experimental setup for measuring the interference signal.

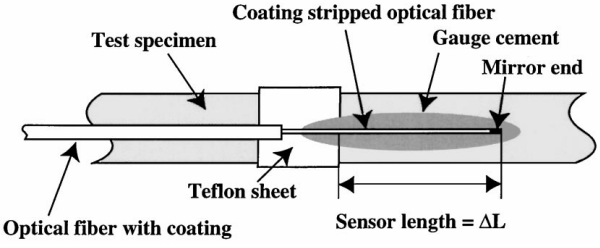

Figure 2 A schematic illustrating control of the sensor length with a Teflon sheet.

An impulse was provided to the test specimen with a hammer used for the Charpy impact test. An impact energy of either 0.06 or 7.3 J was given. The sensor fiber was mounted on the specimen of the opposite side where the hammer hit. The dimensions of the specimen were $80 \times 10 \times 1$ mm^3 and the sensor gauge length, L, was 20.0 mm. Impact load was estimated through a strain gauge mounted on the hammer. The interference signal and load were recorded at a sampling rate of 30,000 samples/s during the impact test.

The tensile test was performed at a cross-head speed of 16.7 μm/s in ambient atmosphere. Load, strain and optical interference signal were recorded at a sampling rate of 1,500 samples/s. Strain was measured with the resistance strain gauge. The sensor fiber with a gauge length of 20.6 mm was mounted on a $180 \times 10 \times 1$ mm^3 specimen with a gauge length of 100 mm. Substituting the sensor gauge length and the properties of the optical fiber into Equation 4, we can obtain the strain sensitivity of the fiber-optic sensor as

$$|\Delta\Phi| = 0.24 \times 10^6 |\varepsilon_z| \quad \text{(rad)} \tag{5}$$

One channel AE measurement was simultaneously performed to evaluate the damage process during the tensile test. An AE sensor (NANO30, PAC) was attached on the specimen on the opposite side of the sensing fiber. The AE signals passed through a preamplifier (1220A, PAC) with a gain of 40 dB were recorded in an AE analyzer (MISTRAS 2001, PAC). The threshold value of AE measurement was set to be 40 dB.

3. Results and discussion

3.1. Sensor response to impact

Figs 3 and 4 show the optical interference signal and load-time curves during the impact test at an impact energy of 0.06 and 7.3 J, respectively. The optical interference signal kept an approximately constant value before impact load was applied. The signal decreased suddenly just when impact load was applied. For the test at an impact energy of 0.06 J, the signal that seemed the sum of two signals with different frequency occurred after impact load was applied. After the impact load decreased to zero, the high-frequency signal with roughly constant amplitude occurred. No damage was observed in the impacted specimen. For the test at an impact energy of 7.3 J, impact load caused the interference signal to oscillate. The amplitude of the oscillation seems to increase after the impact load decreased to zero. The sensing fiber broke at about 6 ms after the impact load was applied and then the signal dropped suddenly to dark current level. The specimen broke into two pieces by the impact.

3.2. Strain and AE behavior during the tensile test

Strain-time curve and AE amplitude during the tensile test is shown in Fig. 5. AE signals with an amplitude over 100 dB are marked at 100 dB owing to the limitation of the AE analyzer. Fig. 6 shows the stress-strain curve along with AE count rate during the tensile test. This tensile test can be divided into the following three stages in terms of damage state.

Stage I: Beginning of the Test—Testing Time at 382 s (Strain: 0–1.18%)

For this stage a small number of AE count rates were recorded and most AE signals had an amplitude under 70 dB. The stress-strain curve showed almost linear relationship. Thus, the damage occurred in this stage must be small scale, such as matrix cracking.

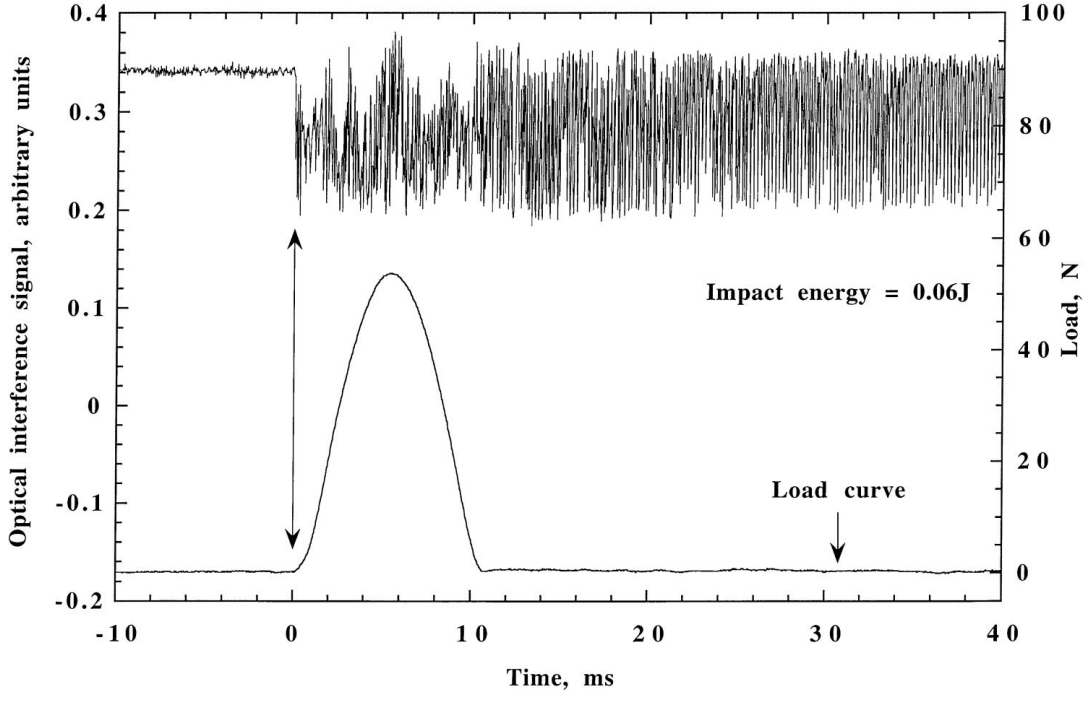

Figure 3 Load and sensor response to hammer impulse at an impact energy of 0.06 J.

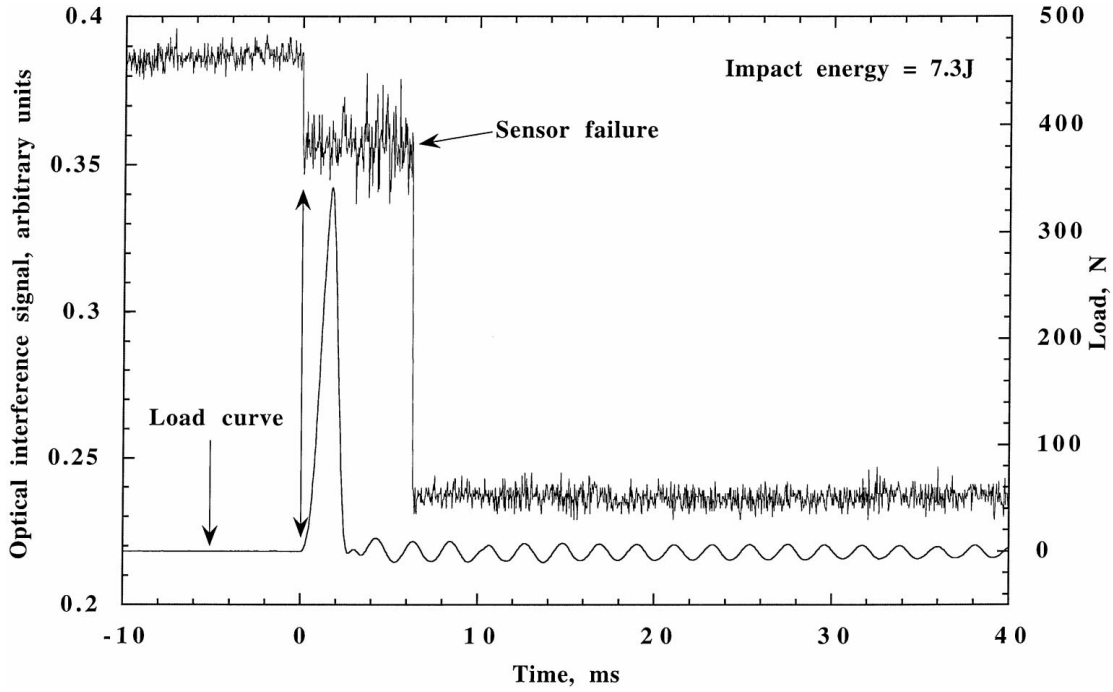

Figure 4 Load and sensor response to hammer impulse at an impact energy of 7.3 J.

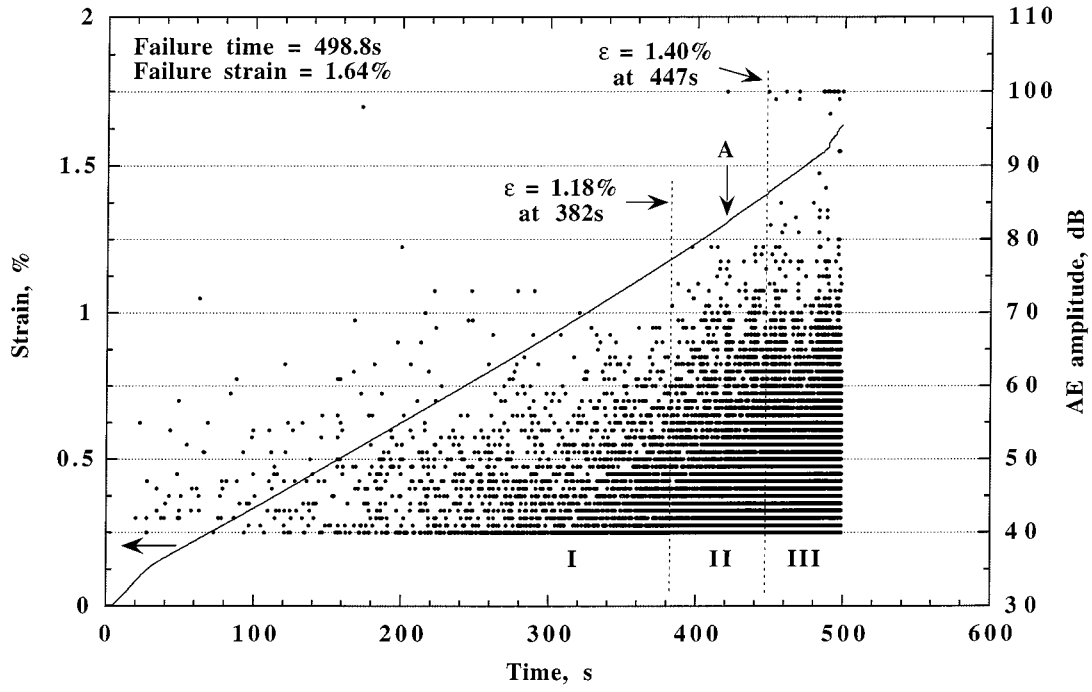

Figure 5 Strain-time curve and AE amplitude during the tensile test.

Stage II: Testing Time at 382–447 s (Strain: 1.18–1.40%)

Many AE signals with an intermediate amplitude from 70 to 80 dB were detected. The stress-strain curve showed almost linear relation except at point A arrowed in Figs 5 and 6. Strain increased suddenly and AE signal with an amplitude of 100 dB was detected at point A. Except point A and just after this, there was no significant difference in AE count rate between stage I and II. In this stage, larger damage compared with the previous stage would occur and some reinforcing fibers would break at point A.

Stage III: Testing Time at 447 s—the End of the Test (Strain: 1.40–1.64%)

Sudden strain increment occurred repeatedly and stress-strain curve showed nonlinear behavior. Some AE signals had an amplitude over 80 dB and high AE count rates were recorded. In this stage, reinforcing fibers would break successively and then the specimen failed.

3.3. Sensor response during the tensile test

The optical interference signal recorded during the tensile test is shown in Fig. 7a along with strain-time curve.

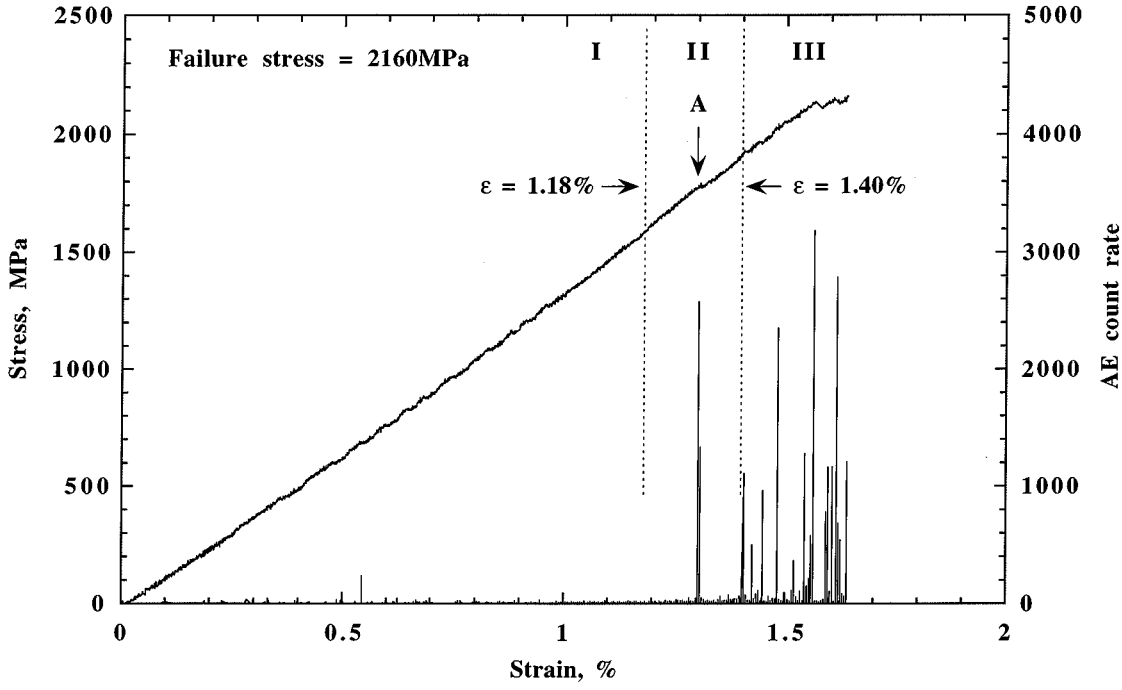

Figure 6 Stress-strain curve and AE count rate during the tensile test.

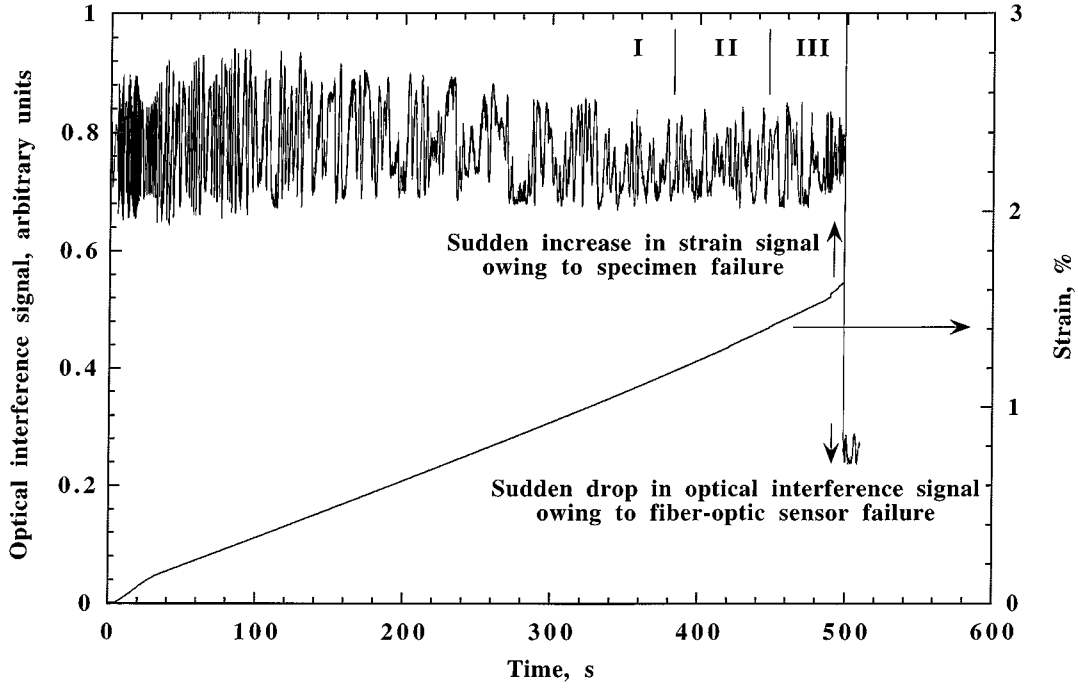

(a)

Figure 7 Optical interference signal and strain-time curve (a) during the tensile test, (b) at the beginning of the tensile test, (c) in Stage III, and (d) the comparison between the optical interference signal and AE count rate in Stage III. (*Continued*).

According to the theoretical relationship between the phase shift in optical interference signal, $\Delta\Phi$, and strain, ε_z, (see Equation 4), the periodical interference signal should occur when strain increases in proportion to time. Except the beginning of the test, however, the optical interference signal demonstrated disordered behavior without periodicity. The fiber-optic sensor failed simultaneously with the specimen fracture and then the interference signal dropped suddenly to dark current level. In the present paper, we note the following two cases in order to investigate the interference signal behavior in detail. One is the beginning of the test where the oscillating signal was recorded. Another is the stage III described in the previous section, where large-scale damage occurred.

Fig. 7b shows the optical interference signal and strain-time curve in the beginning of the tensile test. The interference signal oscillated periodically at a frequency of 0.3 Hz before strain increased. This periodicity would be attributed to the influence of external disturbance such as thermal drift. The interference signal changed discontinuously at point B where strain started to increase. Strain increased linearly with time at a strain speed of 40×10^{-6}/s. Substituting this strain

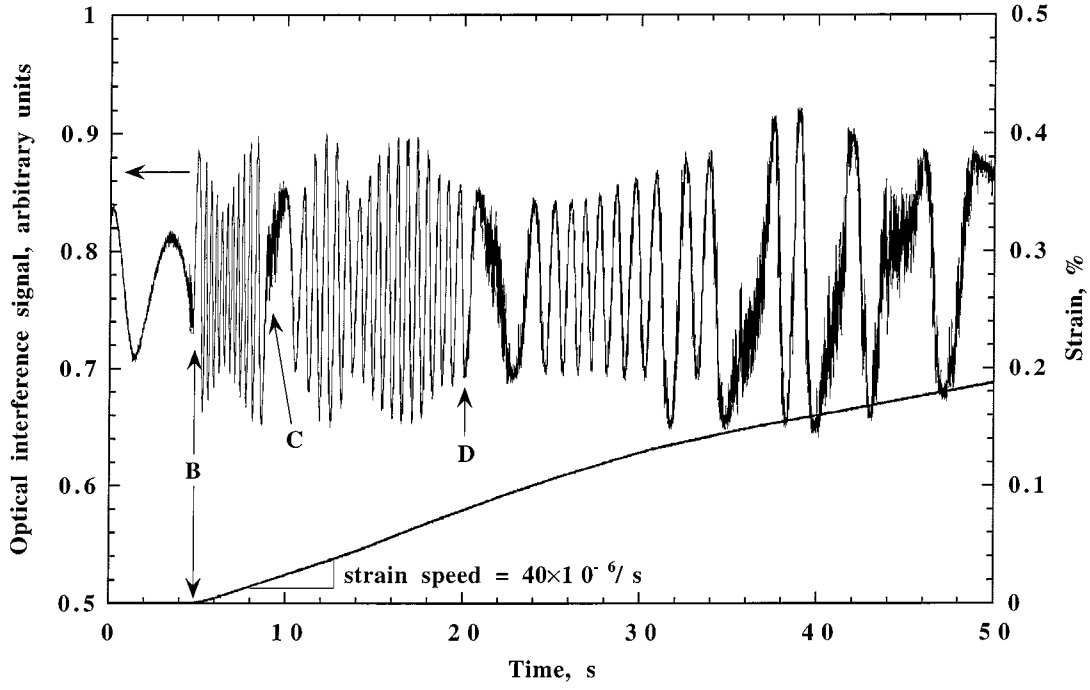

(b)

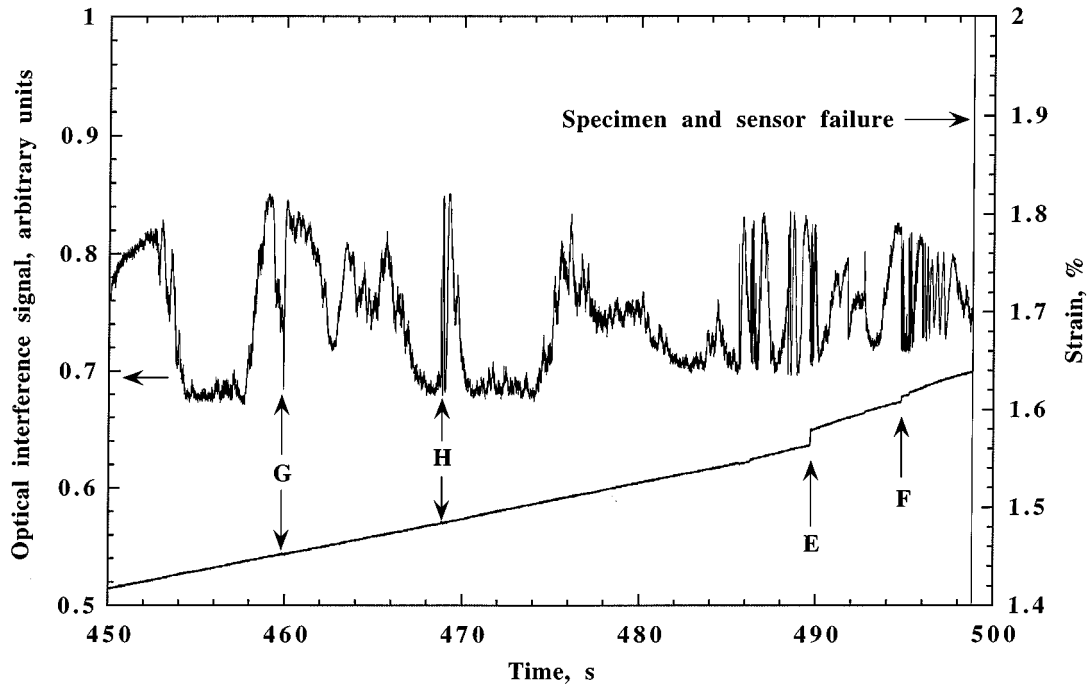

(c)

Figure 7 (*Continued*).

speed into Equation 5, we can calculate the frequency of the interference signal modulated by this steady strain increment to be 1.5 Hz. The measured interference signal after point B, however, periodically oscillated at a frequency of 3 Hz for about 4 s. Then, at point C the high-frequency signal with small amplitude occurred and followed by oscillating signal at a frequency of 1.8 Hz. From point D the high-frequency signal with small amplitude occurred again. The optical interference signal showed different behavior from theoretical prediction.

The first AE signal was detected at a testing time of 20.1 s and its amplitude was 42 dB. This time agreed with point D where the high-frequency interference signal with small amplitude occurred. Small-scale damage detected as small-amplitude AE would disturb the periodical oscillation of interference signal. It can be inferred from the same notion that quite small-scale damage which could not be detected in the present AE measurement would cause the interference signal disorder at point C.

The interference signal and strain-time curve in Stage III where extensive damage occurred is shown in Fig. 7c. The high-frequency interference signal with high amplitude continued for several hundred milliseconds at points E and F. At these points a notable

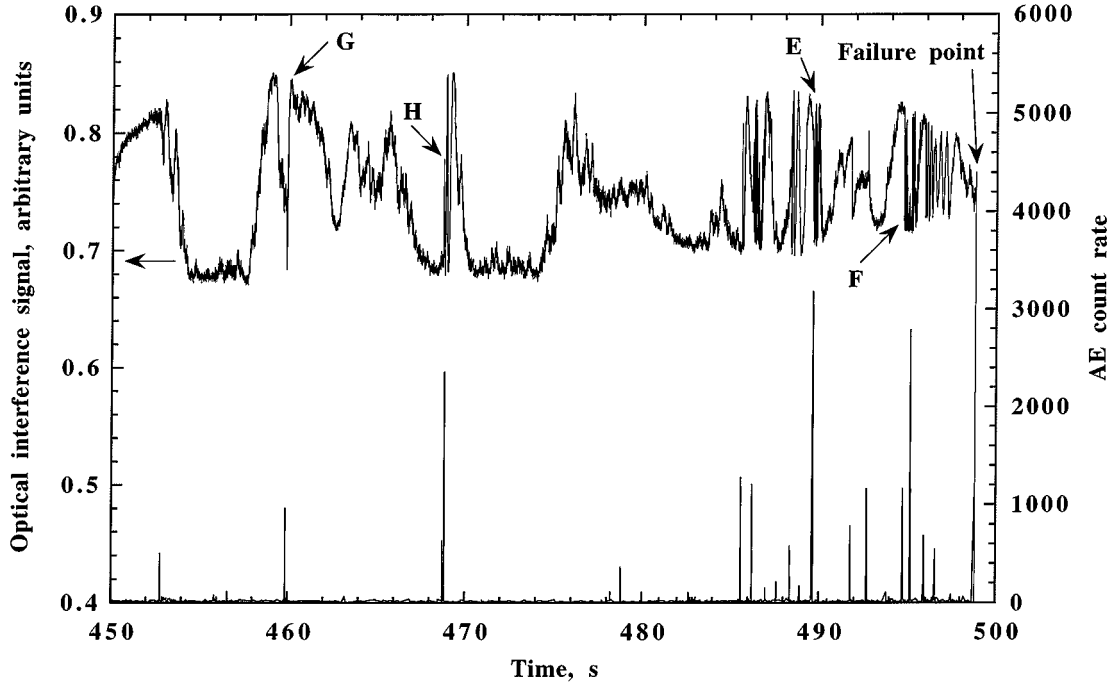

(d)

Figure 7 (*Continued*).

sudden strain increment occurred. Note points G and H where the interference signal changed discontinuously although significant damage was indiscernible from strain-time curve. Fig. 7(d) shows the AE count rate in Stage III along with the interference signal. High AE count rates were recorded at points G and H, so that the significant damage must have occurred at these points. Besides these points, the discontinuous change in the interference signal with high amplitude occurred whenever high AE count rate was recorded.

3.4. Spectrum analysis of the interference signal

The frequency of the interference signal is considered an important parameter for damage detection with interferometric fiber-optic sensors. In the present study, the spectrum analysis of the interference signal recorded during the tensile test was carried out by the Fast Fourier Transforms (FFT). According to the sampling theorem, the highest frequency that can be analyzed is limited to half of sampling rate. The intensity of frequency components up to 750 Hz was estimated since the sampling rate during the tensile test was 1500 samples/s. The intensity of individual frequency component was normalized by the highest-intensity component.

An example of frequency domain representation within the time where no damage would occur is shown in Fig. 8a. For the testing time from 12 to 13 s, no AE signals were detected and the interference signal oscillated periodically (see Fig. 7b). The frequency with the highest intensity was 2 Hz, which corresponded to the frequency of the periodical oscillation occurred then ($\approx$1.8 Hz). Most normalized intensity of the frequency components over 100 Hz ranged from 10^{-6} to 10^{-7}. There are considerable intensity peaks at 14 and 17 Hz. Spectrum analysis performed for a different time span where no AE signals were detected also showed relatively high intensity components at a frequency ranging from 14 to 18 Hz.

Fig. 8b shows the frequency domain diagram of the interference signal during the testing time from 439 to 440 s where some AE signals with an amplitude over 70 dB were detected. The feature of the power spectrum is similar to that of Fig. 8a: the intensity tends to decrease with increasing frequency up to 100 Hz and then ranging within a certain order. Most intensity of frequency components over 100 Hz ranged within an order of 10^{-5}, which is a little higher compared with the previous case.

Fig. 8c shows the frequency domain diagram of the interference signal during the testing time from 489.5 to 490.5 s. This time span covers 0.5 s before and after the large sudden strain increment designated "E" in Fig. 7c. The features of this spectrum differ from the previous two cases. While the intensity tends to decrease with increasing frequency up to 60 Hz, the frequency components from 70 to 100 Hz gain in intensity. Furthermore, most frequency components over 100 Hz had a higher normalized intensity ranging from 10^{-3} to 10^{-4}. In the spectrum analysis performed at a different time span where extensive damage occurred, the frequency components over 100 Hz had a similar intensity.

It can be inferred from the spectrum analysis that the damage signal from interferometric fiber-optic sensors would have a frequency ranging from tens to hundreds Hz. The frequency is quite low compared with that of AE signals, which ranges from tens kHz to 1 MHz. Thus, interferometric fiberoptic sensors are unlikely to detect AE directly. The strain speed at Point E was $2{,}500 \times 10^{-6}$/s. Substituting this strain speed into ε_z of Equation 5, we can estimate the frequency of the interference signal modulated by the sudden strain increment to be 95 Hz. The spectrum diagram shown in Fig. 8c exhibits relatively high intensity at 95 Hz.

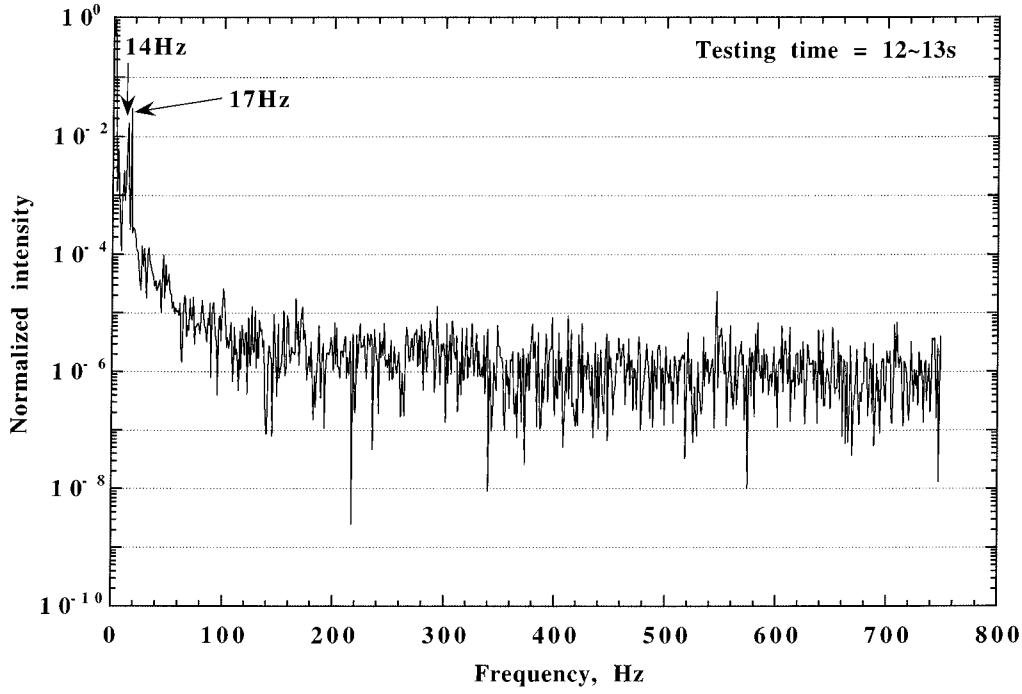

(a)

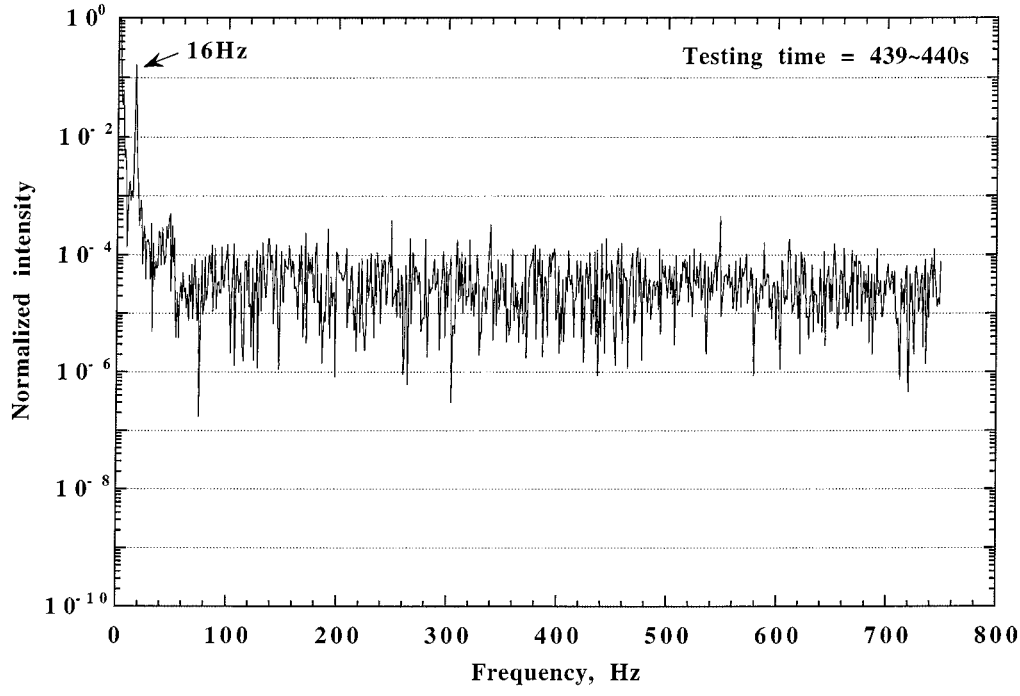

(b)

Figure 8 Frequency domain representation of the interference signal recorded during the testing time from (a) 12 to 13 s, where no AE signals were detected, (b) 439 to 440 s, where some AE signals with an amplitude over 70 dB were detected, and (c) 489.5 to 490.5 s, in which a large sudden strain increment occurred. (*Continued*).

Besides this sudden strain increment, some damage events must have occurred simultaneously and these would cause both displacement and vibration with different strain speeds. Thus, the damage signal whose frequency ranges from tens to hundreds Hz would be induced by both displacement and vibration associated with damage occurrence.

3.5. Real-time damage monitoring

Damage signal from the fiber-optic sensor was extracted by highpass digital filtering. The frequency whose component had relatively high intensity was limited to below 20 Hz when no damage occurred (see Fig. 8a). Hence, the cut-off frequency of the highpass digital filter was set to be 20 Hz. The filtered interference signal is shown in Fig. 9 along with AE count rate. The first remarkable peak appeared at Point I. This time corresponds to point B in Fig. 7b, where strain began to increase. Many significant peaks appeared in the filtered signal near the end of the test. These peaks show a good agreement with damage events where high AE count rate was recorded. Thus, the interferometric fiber-optic sensor can monitor the damage in real time by means of the digital filter.

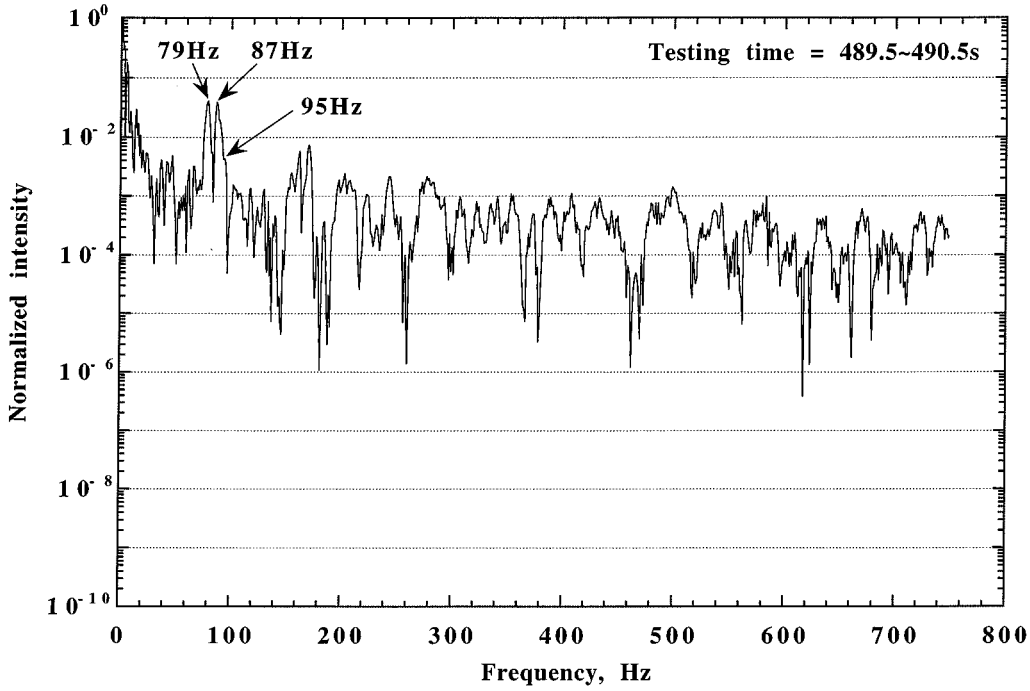

(c)

Figure 8 (*Continued*).

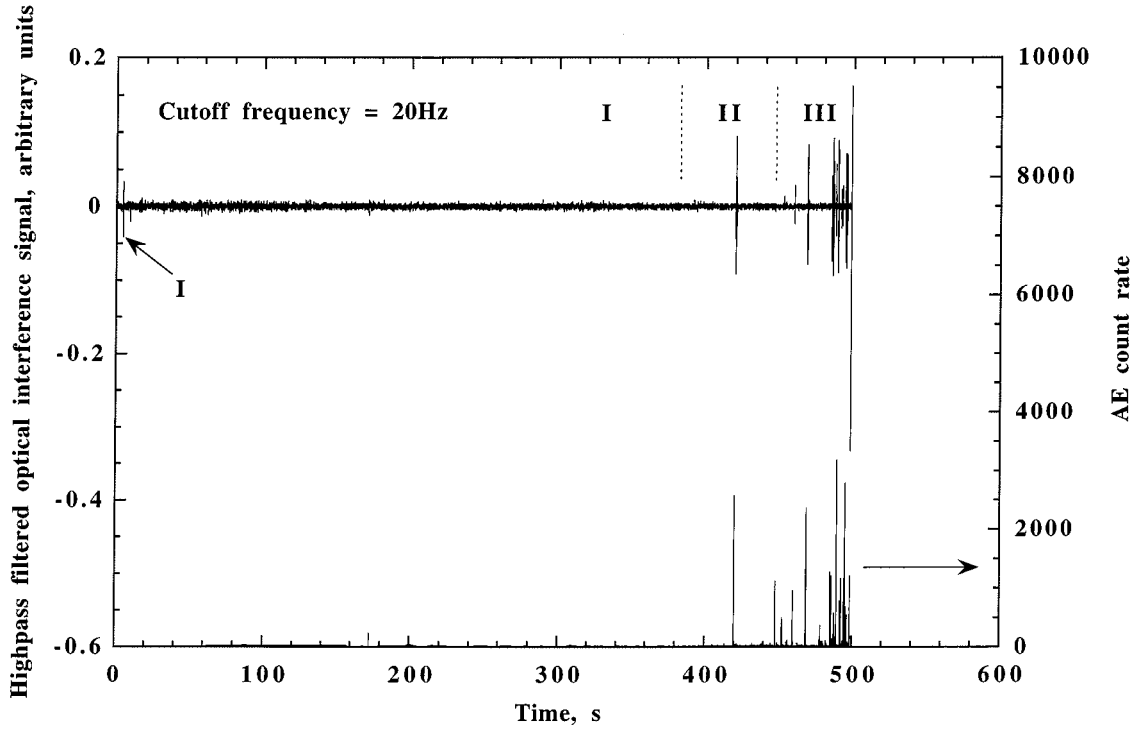

Figure 9 Highpass filtered interference signal and AE count rate during the tensile test.

The significant peaks in the filtered interference signal, however, correspond to only extensive damage events. AE signals with an amplitude of 100 dB were detected at these points, so that extensive fiber breaking must have occurred. As mentioned in the Section 3.3, the interferometric fiber-optic sensor seems to estimate the damage scale from the relative intensity of high-frequency components in the interference signal. Further study is needed to determine the relationship between damage scale and relative intensity of high-frequency components in the interference signal.

4. Conclusions

Damage monitoring of CFRP with a mounted-type Michelson interferometric fiber-optic sensor was investigated. Compared to embedded-type sensors, sensors of this type have the advantage of being exchangeable, and avoiding to reduce the strength of host materials. The following conclusions can be drawn:

(1) The optical interference signal dropped suddenly and followed by high-frequency oscillation when the impact load was applied.

(2) The Michelson interferometric fiber-optic sensor was able to detect the damage by means of the waveform of the interference signal. The high-frequency interference signal with high amplitude occurred when the monitored material was damaged. The intensity of frequency components over 100 Hz increased with the scale of damage.

(3) The damage signal from the interferometric fiber-optic sensor was extracted by highpass digital filtering. The damage signal with high intensity showed a good agreement with damage events detected by AE method. It was shown that the possibility of real-time damage monitoring with fiber-optic sensor through a digital filtering technique.

(4) The mounted-type Michelson interferometric fiber-optic sensor had detected the damage of CFRP up to a strain over 1.5% under tensile loading.

References

1. M. GANDHI and B. THOMPSON, in "Smart Materials and Structures" (Chapman & Hall, London, 1992) p. 70.
2. A. BICOS, in "Fiber Optic Smart Structures," edited by E. Udd (John Wiley & Sons, New York, 1995) p. 629.
3. B. HOFER, *Composites* **18** (1987) 309.
4. S. WAITE, R. TATAM and A. JACKSON, *ibid.* **19** (1988) 435.
5. N. GLOSSOP, S. DUBOIS, W. TSAW, M. LEBLANC, J. LYMER, R. MEASURES and R. TENNYSON, *ibid.* **21** (1990) 71.
6. S. WAITE, *ibid.* **21** (1990) 148.
7. *Idem., ibid.* **21** (1990) 225
8. T. FUKUDA, K. OSAKA and S. KITADE, *J. Soc. Mater. Sci.* Japan **42** (1993) 269.
9. I. KWON, C. KIM and C. HONG, *Compo. Sci. & Tech.* **57** (1997) 1639.
10. C. DOYLE and G. FERNANDO, *J. Mater. Sci. Lett.* **16** (1997) 1104.
11. C. BUTTER and G. HOCKER, *Applied Optics* **17** (1978) 2867.
12. A. BERTHOLDS and R. DÄNDLIKER, *J. Lightwave Tech.* **6** (1988) 17.

Received 20 October 1998
and accepted 3 March 1999